electronics

MDPI

Article

High Frequency and Addressable Impedance Measurement System for On-Site Droplet Analysis in Digital Microfluidics

Jin Zeng, Hang Xu, Ze-Rui Song, Jia-Le Zhou, Guo-Jun Jiang, Bing-Yong Yan *, Zhen Gu * and Hui-Feng Wang

Key Laboratory of Smart Manufacturing in Energy Chemical Process, Ministry of Education, School of Chemistry and Molecular Engineering, East China University of Science and Technology, Shanghai 200237, China; y80200007@mail.ecust.edu.cn (J.Z.); y21210033@mail.ecust.edu.cn (H.X.); y30210988@mail.ecust.edu.cn (Z.-R.S.); zhou.jiale@ecust.edu.cn (J.-L.Z.); jiangguojun@ecust.edu.cn (G.-J.J.); whuifeng@ecust.edu.cn (H.-F.W.)

* Correspondence: byyan@ecust.edu.cn (B.-Y.Y.); guzhen@ecust.edu.cn (Z.G.)

Abstract: Digital microfluidics is a novel technique for manipulating discrete droplets with the advantages of programmability, small device size, low cost, and easy integration. The development of droplet sensing methods advances the automation control of digital microfluidics. Impedance measurement emerges as a promising technique for droplet localization and characterization due to its non-invasive nature, high sensitivity, simplicity, and cost-effectiveness. However, traditional impedance measurement approaches in digital microfluidics based on the high-voltage actuating signal are limited in sensing accuracy in practical applications. In this paper, we propose a novel droplet impedance sensing system for digital microfluidics by introducing a low-voltage and addressable measurement circuit, which enables impedance measurement over a wide frequency range. The proposed measurement system has also been used for detecting the droplet composition, size, and position in a digital microfluidic chip. The improved impedance sensing method can also promote the applications of the digital microfluidic, which requires high accuracy, real-time, and contactless sensing with automatic sample pretreatment.

Keywords: digital microfluidics; impedance measurement; high frequency; addressable; online detection

Citation: Zeng, J.; Xu, H.; Song, Z.-R.; Zhou, J.-L.; Jiang, G.-J.; Yan, B.-Y.; Gu, Z.; Wang, H.-F. High Frequency and Addressable Impedance Measurement System for On-Site Droplet Analysis in Digital Microfluidics. *Electronics* **2024**, *13*, 2810. https://doi.org/10.3390/electronics13142810

Academic Editor: Roald M. Tiggelaar

Received: 11 June 2024
Revised: 10 July 2024
Accepted: 15 July 2024
Published: 17 July 2024

1. Introduction

Digital microfluidics (DMF) is a state-of-the-art fluidic manipulation technique based on electrode arrays, enabling precise control of discrete droplets. It allows manipulating droplets from nanoliter to microliter volumes [1], which has enabled extensive applications in chemistry, biology, and medicine due to its advantages, such as miniaturization, low sample consumption, high efficiency, easy integration, and automation [2]. The DMF chips can function as microreactors for conducting chemical synthesis reactions [3–5]. It has also been developed for biological analysis such as immunoassays [6,7], cell culture [8–11], nucleic acid detection [12–16], and protein analysis [17–20]. Therefore, it has been widely used in the fields of point-of-care testing [21,22], drug screening [23,24], newborn disease screening [25], and clinical diagnosis [22,26]. It is essential to develop a droplet sensing method that enables feedback of the droplet states for fault diagnosis to enhance the control stability of the DMF. Moreover, accessing the physical and chemical properties of droplets can further promote the development of online sensing techniques for DMFs.

Optical imaging and impedance sensing methods are promising to obtain information about droplet position and their physical/chemical properties. Optical imaging using a digital camera is widely applied to detect the states of droplets manipulated on the DMF. It requires an additional optical system and high computing capacity for data processing. In addition, it can hardly provide direct information on the composition of the droplet from the image. As an alternative approach, the impedance-based methods are simple and require

fewer additional elements in the hardware, which has also been widely used for fully automated droplet control [27]. Based on the impedance information, a droplet position can be obtained by measuring differences in individual electrodes [28,29]. Moreover, impedance-based droplet position can be used to diagnose the electrodes [27,29] and to measure the droplet velocity [30,31].

When conducting long-term experiments or chemical reactions on digital DMF chips, real-time monitoring of droplet volume is essential for ensuring the execution of the droplet manipulation, to avoid the negative impact caused by solution evaporation [32,33]. To address the negative impact, Perry et al. [34]. developed a DMF system that integrates an impedance-based adaptive closed-loop water replenishment system with a temperature control system. The system enables the detection of droplet volume and compensates for any evaporated droplet volume, thereby maintaining a consistent assembly reaction concentration during DNA assembly reactions.

Detecting the composition of the droplets on a DMF chip plays a crucial role in distinguishing different solution droplets. This capability enables manipulating, detecting, and analyzing experimental samples in the electrochemical field on DMF chips [35,36]. Using the impedance-measurement-based method, it is possible to distinguish droplets of different concentration solutions [37]. This offers the potential for the automatic dilution of standard solutions.

As reported, the droplet impedance measurement on DMF chips is typically conducted by applying the high-voltage actuating signal on the target electrode as an excitation signal [27–29,34]. Another electrode of the DMF chip serves to detect the response signal. However, due to the high-voltage of the excitation signals, it is challenging to increase the frequency of the excitation signal, which is typically limited to lower than 1 kHz. Consequently, it is hard to achieve droplet impedance measurement at high frequencies. Additionally, the high-voltage AC signal from the booster circuit always contains high noise, leading to low accuracy and poor repeatability in impedance measurement. Due to the low thickness of the dielectric layer in the DMF chip, the high-voltage signal can highly impact the material of the DMF chip, posing a risk of damage to both the DMF chip and the circuit. Furthermore, since the detection circuit relies on resistive voltage division, the circuit itself can introduce signal distortion and exhibit a low input impedance, leading to significant impedance measurement errors.

The conventional DMF droplet impedance measurement and the circuit system face challenges in achieving high-accuracy results and issues from the practical applications. The traditional DMF droplet impedance measurement method is primarily suitable for applications with qualitative purposes and low sensitivity requirements, such as droplet positioning. However, it does not meet the accuracy required for quantitative analysis of droplet physical and chemical properties.

Here, we present a novel impedance measurement system for droplet analysis in DMF by introducing an addressable droplet impedance measurement circuit. The system enables the use of a low AC signal for impedance measurement over a wide frequency range (10 kHz to 60 kHz). Additionally, automatic calibration and real-time data analysis methods are introduced for establishing a highly sensitive detection approach for determining droplet composition, size, and positioning on DMF chips.

2. Materials and Methods

2.1. Detection of Droplet Impedance

A novel configuration of the DMF system is proposed to avoid using a high AC signal as the excitation signal for impedance measurement for high frequency and addressable droplet impedance sensing, as shown in Figure 1. An addressable droplet impedance measurement circuit is designed, where the top plate of the DMF chip is used as the sensing electrode for both the AC signal supply and the response signal detection with a trans-impedance amplifier (TIA). The actuating electrode corresponding to the detection region is grounded during impedance measurement. The excitation signal is a programmable low

AC signal with adjustable frequency, while the response signal is demodulated to obtain the impedance of the droplet over a wide frequency range. Automatic calibration and real-time data analysis methods are executed to inform the droplet composition, size, and positioning on the DMF chip.

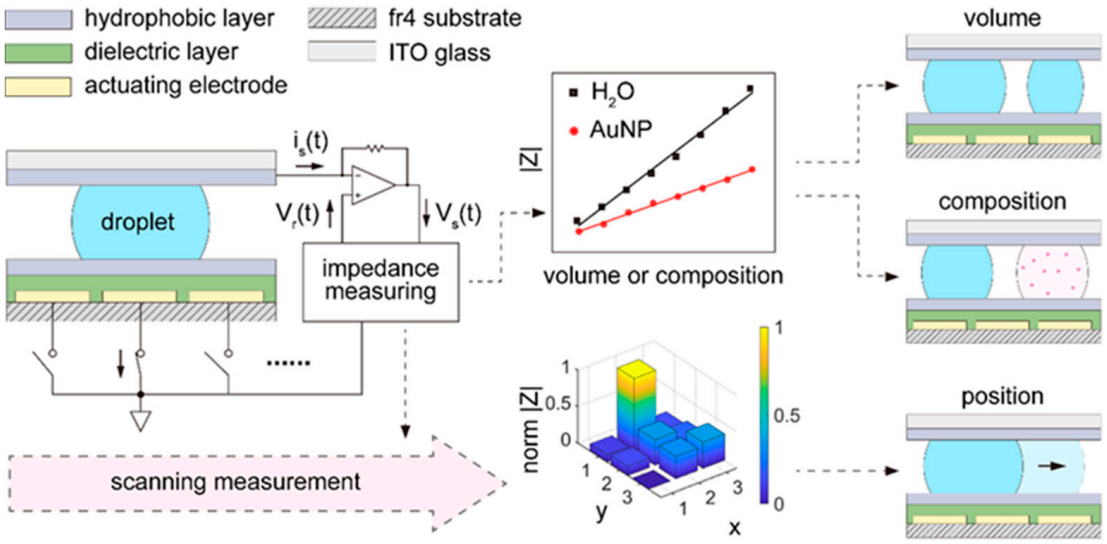

Figure 1. Schematic diagram of the proposed digital microfluidics droplet impedance measurement method in this paper.

2.2. Equivalent Circuit Model

The circuit of the electrowetting-on-dielectric (EWOD)-based DMF can be described as a combination of capacitive components [38]. Therefore, the equivalent circuit model of the single electrode on the DMF chip can be established, as shown in Figure 2. The equivalent circuit model of the DMF is a network of resistance and capacitance, in which the droplet can be modeled as a parallel circuit of resistance and capacitance. The air and hydrophobic layer are equated to a capacitive component. On a DMF chip, the gap between the top and bottom plate is much smaller than the electrode size. Each equivalent capacitance can be considered as a parallel plate capacitance. The droplet can be approximated as a cylinder.

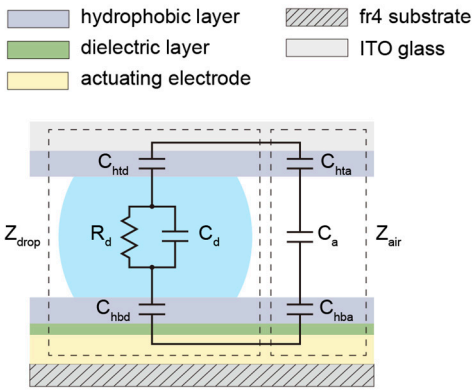

Figure 2. Equivalent circuit model of the DMF system. Z_{drop} is the equivalent impedance of the droplet on the hydrophobic layer (C_{htd}, C_{hbd}). Z_{air} is the equivalent impedance of the air, where the hydrophobic layer (C_{hta}, C_{hba}) is not in contact with the droplet.

For the gap distance d and the electrode area A, the equivalent resistance and equivalent capacitance are as follows:

$$R = \frac{\rho d}{A} \, C = \frac{\varepsilon A}{d}, \tag{1}$$

where ρ is the resistivity, and ε is the dielectric constant.

The equivalent impedance of the electrode with a droplet can be described as follows:

$$Z_{drop} = Z_d + Z_{htd} + Z_{hbd} = \frac{c_{drop}}{A_e x_{drop}}, \tag{2}$$

where x_{drop} represents the ratio of the overlapped area of the droplet and a certain electrode to the area of the electrode.

The equivalent impedance of the part without a droplet is as follows:

$$Z_{air} = Z_a + Z_{hta} + Z_{hba} = \frac{c_{air}}{A_e\left(1 - x_{drop}\right)}. \tag{3}$$

The total impedance is as follows:

$$Y_{tot} = \frac{1}{Z_{tot}} = \frac{1}{c_{drop}c_{air}d} \times \left[\left(c_{air} - c_{drop}\right)V_{drop} + c_{drop}A_e d\right], \tag{4}$$

where $V_{drop} = x_{drop}A_e d$ is the volume of the droplet. As the frequency of the excitation signal in impedance sensing has a certain value, ω, c_{drop}, and c_{air} are regarded as constants. Therefore, there is a linear relationship between the reciprocal of the impedance value, the electrode area, and the droplet volume.

2.3. Design and Fabrication of DMF Chip

The DMF chip consists of two plates: the bottom layer is made of a printed circuit board (JLCPCB, Shenzhen, China), which contains 19 actuation electrodes (2.25 mm × 2.25 mm, with a zigzag edge), two reservoir electrodes (9.72 mm × 6.95 mm), and a common electrode with gold plating technology. A 10 μm-thick polytetrafluoroethylene (PTFE) film (Hongfu Material, Dongguan, China) was attached to the top of the electrodes as a dielectric layer and a superhydrophobic layer. The top plate was an indium tin oxide (ITO) glass with a thickness of 1.1 mm and a square resistance of approximately 8 Ω. A Cytop film (CTX-809SP2, AGC Inc., Tokyo, Japan) was spin-coated on the ITO glass to act as a hydrophobic layer for the top plate. A conducting tap was soldered onto the bottom electrode to maintain the space (~1.6 mm) between the two plates. All the electrodes were led out using pin headers in order to connect with external devices.

2.4. Design of the DMF System

As shown in Figure 3a, a custom-designed DMF system was applied to manipulate droplets and conduct impedance measurements. The system comprised an electronic control board and an impedance measurement circuit. The electronic control board had a charge pump circuit capable of generating high-voltage ranging from 60–300 V. It enabled the switching of actuation electrodes between high-voltage ground and floating states and the switching of the top plate between ground and excitation states for impedance measurement using an optocoupler switch circuit.

The impedance measuring is realized based on a measurement circuit and a calibration circuit. The impedance measuring was implemented using an integrated net analyzer (AD5933, Analog Devices Inc., Dallas, TX, USA), which applied excitation signals to the top plate and measured the response signals on the corresponding electrode. The calibration circuit was a multiplexer (ADG708, Analog Device Inc., Dallas, TX, USA), which could switch the input and output between the measuring system and standard resistors.

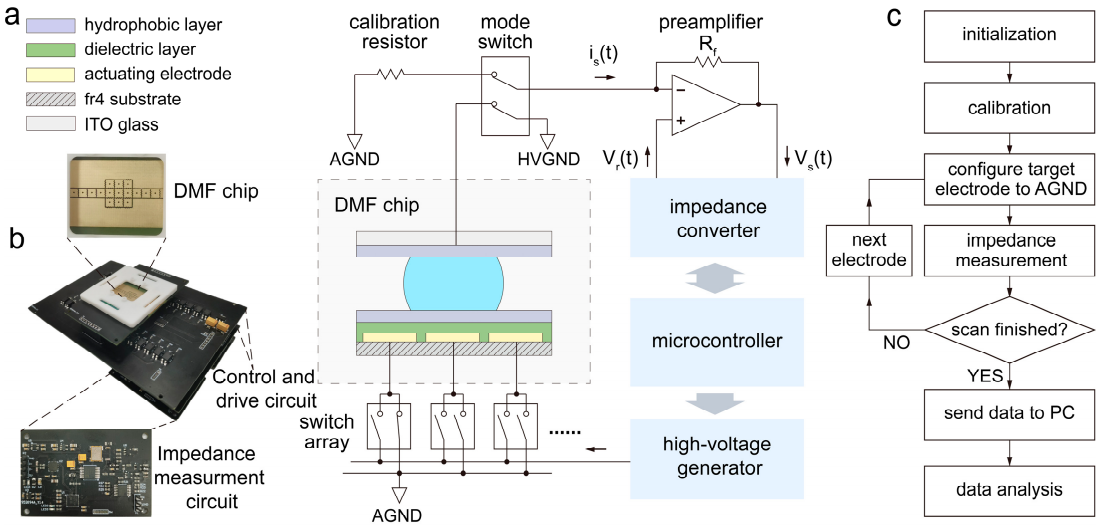

Figure 3. The principle and process of droplet impedance measurement. (**a**) Schematic diagram of impedance measurement for a single droplet on a DMF chip; (**b**) System physical diagram; (**c**) Impedance measurement process flowchart.

2.5. Measurement of Droplet Impedance

The setup for impedance measurement is shown in Figure 3c. First, the system is initialized, and the impedance measurement parameters are set, including the settings of the amplitude, frequency, and number of excitation detections. Secondly, set the selection of standard resistors for calibration according to the approximate range of impedance to be measured and the calculation of the system gain coefficient G:

$$G = \frac{1}{(A_c - A_0) \times R_c}, \tag{5}$$

where A_0 is the amplitude of the AC excitation signal, and A_c is the amplitude of the measured signal with the calibration resistor R_c. Since the system gain coefficient G will be affected by the excitation signal, calibration should be performed again when the excitation signal changes. The standard resistor used for calibration is as close as possible to the range of impedance to be measured to minimize detection errors. After calibration, set the target electrode to be grounded for impedance measurement, set the rest of the electrodes to float, and perform droplet impedance measurement with the set parameters. After detecting all the electrodes on the DMF chip, the data will be sent to the PC for processing and analysis, which includes impedance calculation $|Z|$:

$$|Z| = \frac{1}{G \times (A_m - A_0)}. \tag{6}$$

In Equation (6), A_m is the amplitude of the impedance response signal to be measured.

2.6. Circuit Simulation

LTspice (Analog Device Inc., Wilmington, MA, USA) was used to perform the simulation of impedance sensing. A series of droplets with different volumes were simulated and compared with the measurement results of actual experiments to verify the reasonableness of the structural parameter settings of the equivalent circuit model. The simulation circuit is constructed based on the equivalent circuit model of the digital microfluidic system and the measurement circuit (Figure 4). Parameters in the model of the DMF chip (Table 1) are listed in Table 1. During simulation, a set of sinusoidal signals with biased voltage were generated as excitation signals by a voltage source. Water droplets were selected as the object of simulation, and a series of droplets with a droplet volume ratio (the ratio of

droplet volume to the volume between a single electrode and the upper pole plate on the DMF chip) ranging from 0.1 to 0.8 were selected for the experiments. A 10 kHz sinusoidal signal with an amplitude of 2.0 V and a DC bias of 1.48 V is used as the excitation signal, and the waveforms of the excitation and response signals were recorded and analyzed.

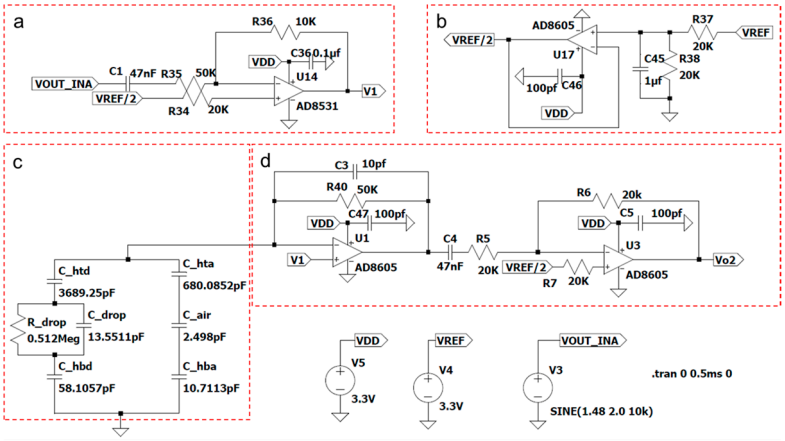

Figure 4. The simulation model of the impedance measurement circuit. (**a**) excitation signal adjustment circuit; (**b**) DC bias voltage generation circuit; (**c**) equivalent circuit model of the digital microfluidic system; (**d**) analog front circuit for impedance measurement.

Table 1. Electrical and geometric parameters used in equivalent circuit model simulations and real-world experiments.

Material	Relative Permittivity ε_r	Resistivity ρ (Ω·m)	Thickness d
Air	1.0	2.0×10^{14}	1.6 mm
Water	80.1	1.8×10^{5}	1.6 mm
Top hydrophobic (Cy-top)	2.0	1.0×10^{15}	0.15 μm *
Bottom hydrophobic (Teflon)	2.1	1.0×10^{16}	10 μm

* The thickness of the hydrophobic layer of the upper pole plate is estimated based on the Cytop spin coating thickness curve and spin coating parameters.

3. Results and Discussion

3.1. Validation of the Impedance Model

The circuit simulation and droplet impedance measurement were conducted to validate the proposed impedance model for the DMF chip with droplets. To make the results between the simulation and the experiment comparable, a linear function normalization (Min-Max Scaling) method is adopted to map the data to a range between 0 and 1. The droplet proportion x_{drop} was defined as the ratio of the droplet volume V_{drop} to the individual electrode volume $A_e d$.

$$x_{drop} = \frac{V_{drop}}{A_e d} \tag{7}$$

where A_e is the individual electrode area, and d is the gap distance.

As shown in Figure 5, the simulated data were well fit to the experimental data, which supports that the circuit model for the DMF chip with droplets is reasonable. In other words, the equivalent circuit model can serve as a theoretical reference for droplet impedance measurement. Meanwhile, it also reveals that factors such as the curvature of the droplets and wire impedance have limited influence on the measurement result. It suggests that our proposed impedance sensing method based on excitation signals with low voltage and high frequency is suitable for the measurement of droplet impedance.

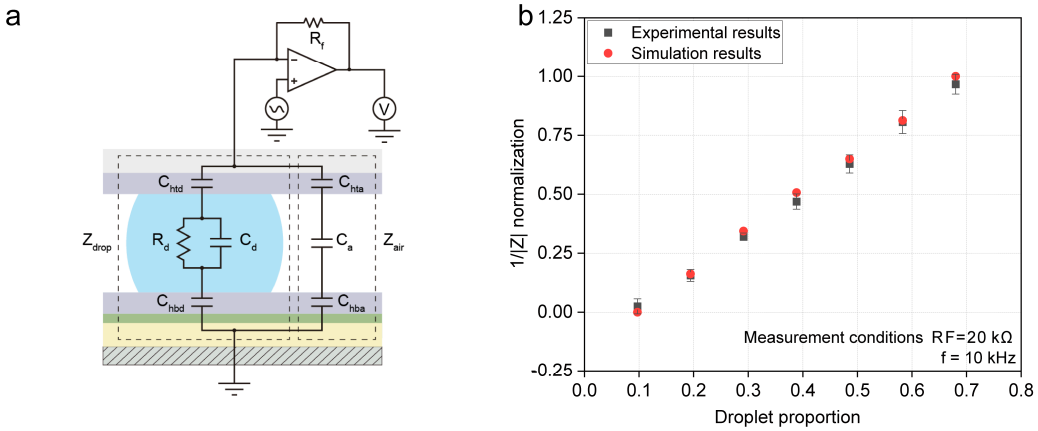

Figure 5. (**a**) The equivalent circuit model of the droplet in a DMF chip. (**b**) Normalized results of the simulation and experiment with different droplet proportions (n = 5).

3.2. Droplet Positioning

Testifying the accuracy of the impedance measurement for droplet positioning, a droplet (20 µL, de-ionized water) was loaded into a 3 × 3 DMF electrode array. As shown in Figure 6, the droplets were manipulated to move to different locations on the electrode array, which can be classified into two conditions according to the droplet center: 1. on the center of an electrode (Figure 6a) and 2. at the gap between two electrodes (Figure 6b,c). An impedance scanning process was executed by switching the electrodes to ground one by one and recording the corresponding impedance value using custom-designed software. The reciprocal of the impedance was calculated and normalized (Norm (1/|Z|)) to visualize the impedance information of the electrode array. The obtained impedance results were then imported into MATLAB(R2023b) for further processing. According to the 3D image of the impedance data, as shown in Figure 6a, it is obvious that a high Norm (1/|Z|) was obtained when the droplet overlapped with the corresponding electrode. In this study, we employ three methods to determine the droplet position: thresholding, support vector machine (SVM) classification, and thresholding after data normalization. The accuracy of these three methods is compared, and the method with the highest accuracy was selected for droplet position recognition.

The thresholding method involves selecting a suitable value based on the difference between the impedance of the electrodes with/without a droplet. When the impedance measured on a certain electrode was higher than the threshold value, it is considered that a droplet was on that electrode, otherwise, no droplet was on that electrode. The SVM was a classic method for coordinate classification. Here, it was used to classify and recognize the condition of the droplets based on a test set of 100 samples. During position, the trained SVM model was used to verify if the droplet was located on the electrode. Then the position of the droplets was further estimated according to the classification result of each electrode in the array. The method of thresholding after data normalization involves linearly normalizing the impedance data and mapping it to the range between 0 and 1. To evaluate the three methods, samples with different droplet conditions were acquired. For each sample, the impedance of each electrode in the array (3 × 3) was first used to verify the presence of a droplet on the electrode. Then the droplet condition can be informed based on the states of the electrode array. As a result, the method of thresholding after data normalization achieved the highest accuracy of 93.75% (Figure 6d). The accuracy of SVM and the threshold method were lower than 60%. The low accuracy of the two methods may result from the fluctuation of the absolute value of the impedance as the droplet may have different overlapped areas with the electrodes even at the same condition. When the droplet is located in the center of the target electrode with few overlapped areas on the neighbor electrodes, it appears to have a high impedance on the target electrode and a low impedance on the neighbor electrodes. In practice, the droplet position could

be biased from the electrode center, resulting in an increase in the overlapped area on neighboring electrodes and affecting the impedance. Although the threshold method is fast and easy to realize, it is hard to find a fixed threshold suitable for droplet position in each measurement. For the SVM, it requires learning from prior data. In addition, the fluctuation of the range of impedance value also makes it hard to classify the state of each electrode. The normalized method makes the impedance value comparable between different measurements, as shown in Figure 6a–c for different droplet positions.

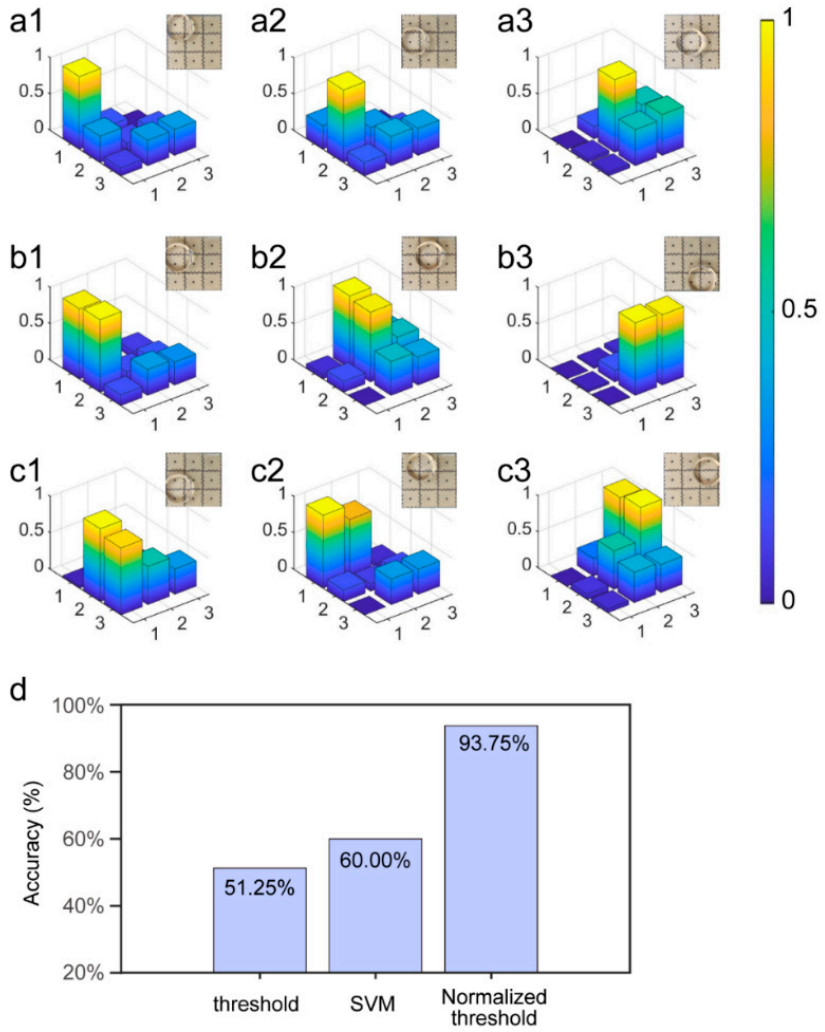

Figure 6. Results of the droplet localization experiments. (**a**) is the impedance of the electrode array when the droplet center is located in the center of an electrode; (**b**,**c**) are the impedance of the electrode array when the droplet center is located at the edge of two electrodes; (**d**) is the accuracy of the three methods for droplet positioning.

3.3. Detection of Droplet Volume

According to the equivalent circuit model, there is a positive linear relationship between the volume of droplets and the reciprocal of impedance Y_{tot}. In order to verify this in practice, droplets of NaCl solution (1 mol/L) with volume ratios in the range of 0 to 0.8 were used for impedance detection. The amplitude of the excitation signal was set to 0.4 V with frequency ranging from 10 kHz to 60 kHz at a step of 10 kHz. After the impedance measurement of the droplet with different volumes, curve fitting was performed to verify the linearity of the droplet volume and the impedance. As a result, the Y_{tot} has a good linearity with the droplet volume ratio (Figure 7). All the R^2 values of the linear fitting at different frequencies were higher than 0.99. It also reveals that the slope of the linear regression

increases with increasing frequency of the excitation signal. Therefore, it suggests that the sensitivity of impedance detection for digital microfluidics can be enhanced by increasing the frequency of the excitation signal.

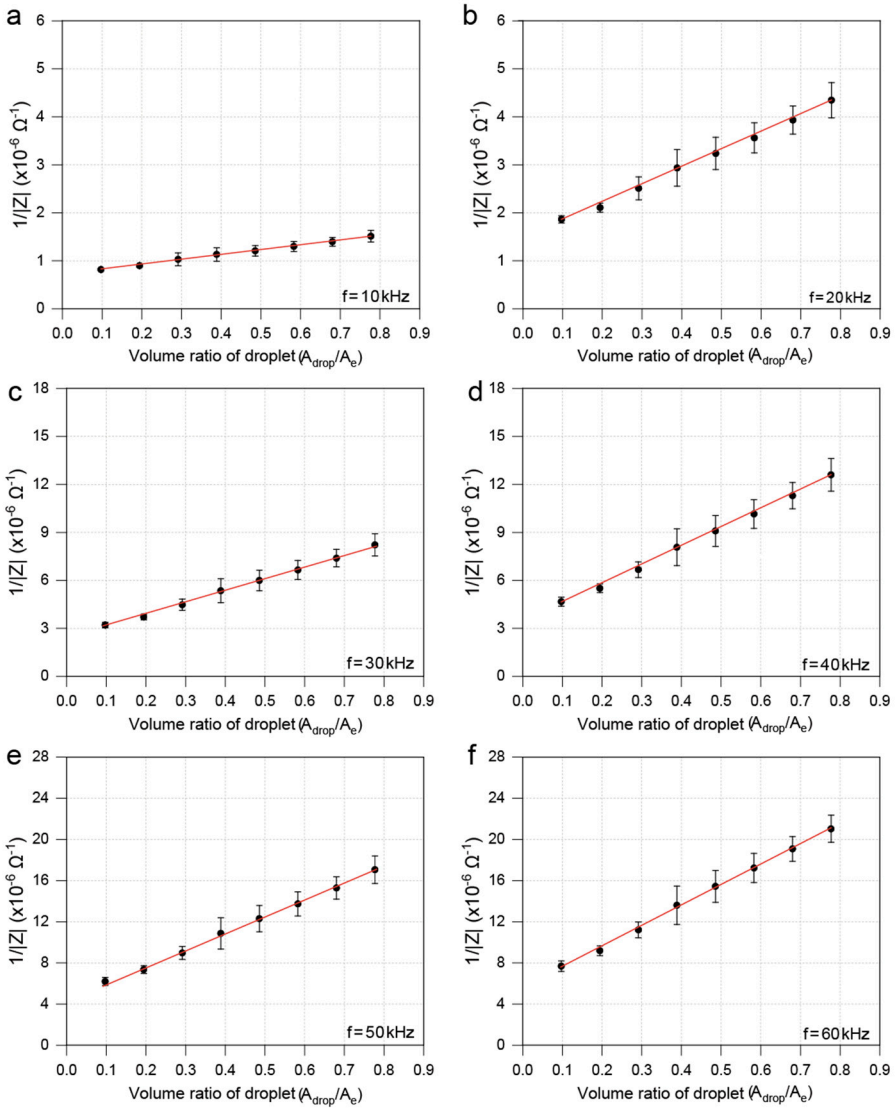

Figure 7. Droplet volume measurement results of 1 mol/L NaCl solution. (**a**–**f**) represent plots of the volume ratio of droplet and impedance reciprocal in different frequencies (10 kHz, 20 kHz, 30 kHz, 40 kHz, 50 kHz, and 60 kHz) (n = 5).

3.4. Detection of Droplet Composition

As the dielectric constants and resistivities of a droplet depend on its compositions, it is theoretically possible to distinguish droplets with different compositions by their impedance. Here, droplets of de-ionized (DI) water and gold nanoparticles (AuNP) were introduced to evaluate the capacity of the proposed method for composition analysis. Each experiment consisted of measurements of 8 droplets with different volumes. The excitation signal was set to an amplitude of 0.4 V with frequency ranging from 10 kHz to 60 kHz.

As shown in Figure 8, the impedance with droplets of DI water and AuNP (gold nanoparticles) from five repeated experiments was acquired. The relationship between droplet volume and the Y_{tot} exhibited a consistent positive linear relationship. However, at the same frequency, the slopes of the linear regression were different for droplets with different compositions. As shown in Figure 8, within the frequency range of 10 kHz to 60 kHz, the impedance of droplets from DI water and AuNP solutions could not be

effectively differentiated at 20 kHz. However, at 60 kHz, the impedance of droplets from DI water and AuNP solutions exhibited the most distinct differences, indicating that a specific frequency is required for optimal discrimination of a particular solution. Therefore, it suggested that droplets with different composition can be distinguished based on impedance measurement with a suitable frequency of the excitation signal.

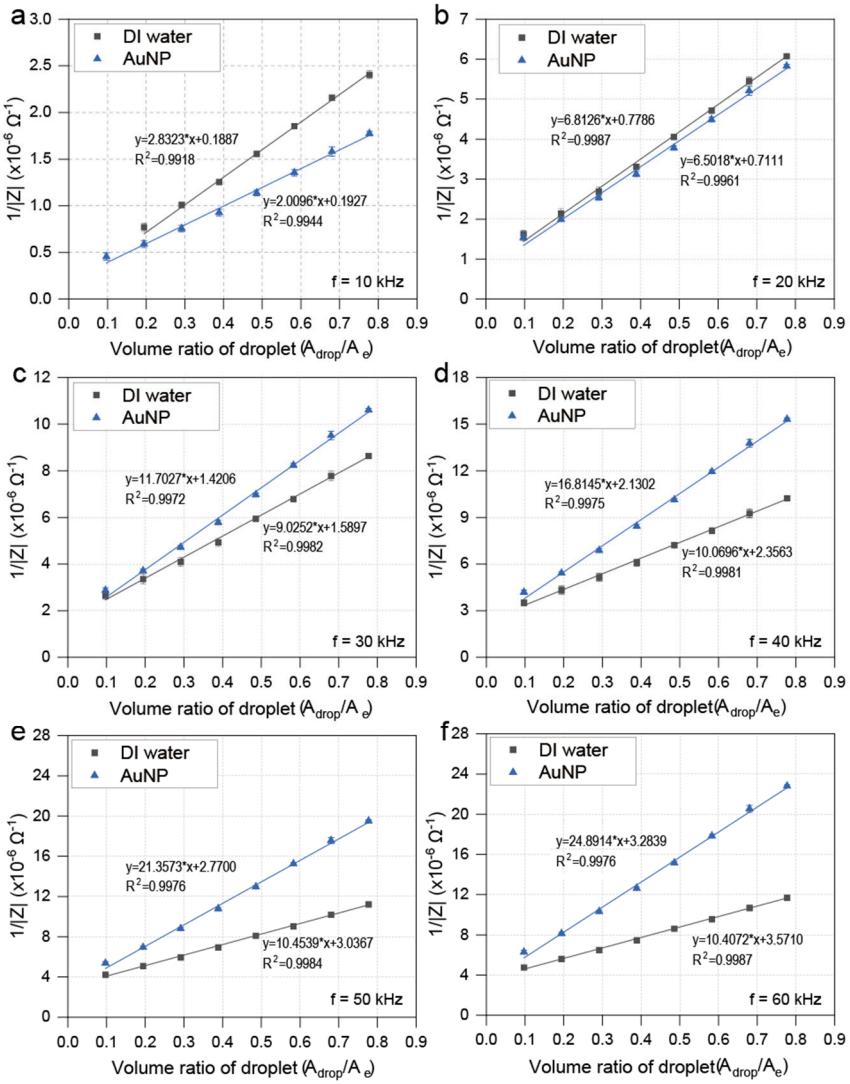

Figure 8. Impedance measurement of droplets with DI water and AuNP at different volumes. (**a**–**f**) represent plots of the volume ratio of droplet and impedance reciprocal in different frequencies of AuNP and DI water (10 kHz, 20 kHz, 30 kHz, 40 kHz, 50 kHz, and 60 kHz) (n = 5).

3.5. Detection of Salt Concentration

The system was further used to measure the impedance of droplets with different NaCl concentrations ranging from 1 µmol/L to 10^6 µmol/L. In the experiment, droplets with a volume of 20 µL were added to the DMF chip and moved to the center of the same electrode. The amplitude of the excitation signal was 400 mV, and the impedance was measured at frequencies of 10 kHz and 20 kHz. Each condition in the experiment was repeated five times. As a result, the droplet impedance rises with the increase of the salt concentration (Figure 9). The change of the impedance was significant at the concentration range from 1 µmol/L to 10^3 µmol/L, while the change of impedance reached a plateau when the salt concentrations were higher than 10^4 µmol/L. This could be due to the detection limit of the impedance. With the increase of the salt concentration, the capacitance of the droplet increases, but the resistance of the droplet decreases. The impedance of the droplet depends

on its capacitance and resistance. Therefore, after a certain concentration, the change of the impedance caused by the concentration increase becomes not obvious compared with the impedance of the whole system. The experimental results indicate that within a certain concentration range, the proposed impedance sensing can be used to determine the salt concentrations. Although the impedance is not linear to the NaCl concentration, the NaCl concentration can still be discriminated based on the impedance even between the low concentration range (1–10 μmol/L). In addition, the impedance response to the concentration varies with the frequency, which will provide more information using multi-frequency detection. Therefore, the proposed method can be further developed for rapid qualitative and semi-quantitative analysis of droplet composition based on a nonlinear calibration method such as look-up table or supervised machine learning.

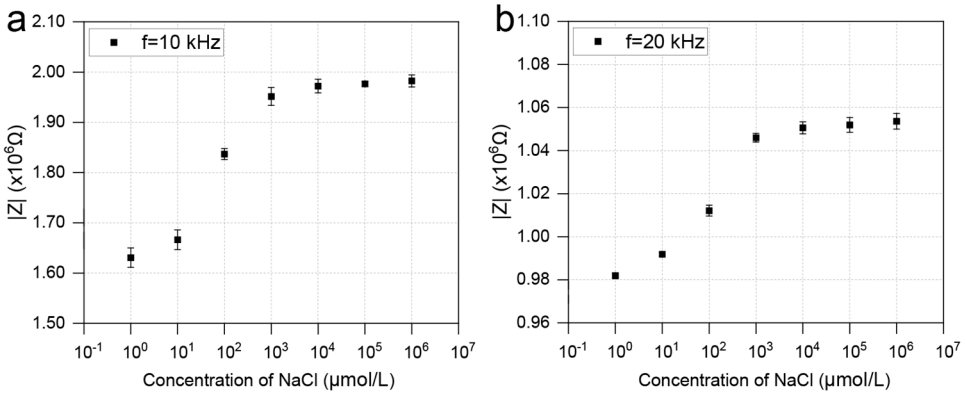

Figure 9. Impedance measurement of droplets with different salt concentrations at frequencies of 10 kHz (**a**) and 20 kHz (**b**) (n = 5).

4. Conclusions

This paper proposes a novel DMF impedance-based droplet analysis method by constructing an addressable droplet impedance measurement system with a low voltage of excitation signals. The proposed system enables impedance measurement over a wide frequency range. An equivalent circuit model was established for digital microfluidics chips and validates the rationality of the model structure and parameter settings through simulations, thereby providing a theoretical basis for impedance formulas derived from the equivalent circuit model for droplet impedance measurement. Based on the proposed impedance measurement method, a custom-designed DMF system was developed, and a series of droplet impedance measurement experiments were conducted to demonstrate its ability to detect droplet position, size, composition, and salt concentration. It can be widely used in application of digital microfluidics that require feedback droplet control, contactless sensing, and small device size.

Author Contributions: J.Z.: investigation, methodology, data analysis, and writing-original draft; H.X.: data analysis and writing-original draft; Z.-R.S.: investigation, methodology, data analysis, and writing-review & editing; J.-L.Z.: investigation and writing-review & editing; B.-Y.Y.: investigation and writing-review & editing; G.-J.J.: investigation and writing-review & editing; Z.G.: conceptualization, methodology, writing-original draft, and supervision; H.-F.W.: conceptualization, writing-review and editing, and supervision. All authors have read and agreed to the published version of the manuscript.

Funding: This research was funded by the National Key R&D Program of China (2021YFC2101101) and the National Natural Science Foundation of China (No. 62103148).

Data Availability Statement: Data are contained within the article.

Conflicts of Interest: The authors declare no conflicts of interest.

Abbreviations

DMF: Digital microfluidics; PCR, Polymerase Chain Reaction; POCT, Point of Care Testing; DNA, Deoxyribose Nucleic Acid; AC, Alternating Current; DC, Direct Current; EWOD, Electro-wetting on Dielectric; PCB, Printed Circuit Board; PTFE, Polytetrafluoroethylene; ITO, Indium Tin Oxide; SVM, Support Vector Machine.

References

1. Geng, H.; Feng, J.; Stabryla, L.M.; Cho, S.K. Dielectrowetting manipulation for digital microfluidics: Creating, transporting, splitting, and merging of droplets. *Lab Chip* **2017**, *17*, 1060–1068. [CrossRef] [PubMed]
2. Li, J.; Kim, C.C. Current commercialization status of electrowetting-on-dielectric (EWOD) digital microfluidics. *Lab Chip* **2020**, *20*, 1705–1712. [CrossRef] [PubMed]
3. Jebrail, M.J.; Bartsch, M.S.; Patel, K.D. Digital microfluidics: A versatile tool for applications in chemistry, biology and medicine. *Lab Chip* **2012**, *12*, 2452–2463. [CrossRef] [PubMed]
4. Ahmadi, F.; Simchi, M.; Perry, J.M.; Frenette, S.; Benali, H.; Soucy, J.P.; Massarweh, G.; Shih, S.C.C. Integrating machine learning and digital microfluidics for screening experimental conditions. *Lab Chip* **2022**, *23*, 81–91. [CrossRef] [PubMed]
5. Jebrail, M.J.; Ng, A.H.; Rai, V.; Hili, R.; Yudin, A.K.; Wheeler, A.R. Synchronized synthesis of peptide-based macrocycles by digital microfluidics. *Angew. Chem. Int. Ed. Engl.* **2010**, *49*, 8625–8629. [CrossRef] [PubMed]
6. Wang, Y.; Ruan, Q.; Lei, Z.C.; Lin, S.C.; Zhu, Z.; Zhou, L.; Yang, C. Highly Sensitive and Automated Surface Enhanced Raman Scattering-based Immunoassay for H5N1 Detection with Digital Microfluidics. *Anal. Chem.* **2018**, *90*, 5224–5231. [CrossRef] [PubMed]
7. Shamsi, M.H.; Choi, K.; Ng, A.H.; Wheeler, A.R. A digital microfluidic electrochemical immunoassay. *Lab Chip* **2014**, *14*, 547–554. [CrossRef] [PubMed]
8. Xu, X.; Cai, L.; Liang, S.; Zhang, Q.; Lin, S.; Li, M.; Yang, Q.; Li, C.; Han, Z.; Yang, C. Digital microfluidics for biological analysis and applications. *Lab Chip* **2023**, *23*, 1169–1191. [CrossRef] [PubMed]
9. Eydelnant, I.A.; Uddayasankar, U.; Li, B.; Liao, M.W.; Wheeler, A.R. Virtual microwells for digital microfluidic reagent dispensing and cell culture. *Lab Chip* **2012**, *12*, 750–757. [CrossRef]
10. Shih, S.C.; Barbulovic-Nad, I.; Yang, X.; Fobel, R.; Wheeler, A.R. Digital microfluidics with impedance sensing for integrated cell culture and analysis. *Biosens. Bioelectron.* **2013**, *42*, 314–320. [CrossRef]
11. Tong, Z.; Shen, C.; Li, Q.; Yin, H.; Mao, H. Combining sensors and actuators with electrowetting-on-dielectric (EWOD): Advanced digital microfluidic systems for biomedical applications. *Analyst* **2023**, *148*, 1399–1421. [CrossRef] [PubMed]
12. Narahari, T.; Dahmer, J.; Sklavounos, A.; Kim, T.; Satkauskas, M.; Clotea, I.; Ho, M.; Lamanna, J.; Dixon, C.; Rackus, D.G.; et al. Portable sample processing for molecular assays: Application to Zika virus diagnostics. *Lab Chip* **2022**, *22*, 1748–1763. [CrossRef] [PubMed]
13. Coelho, B.J.; Veigas, B.; Bettencourt, L.; Águas, H.; Fortunato, E.; Martins, R.; Baptista, P.V.; Igreja, R. Digital Microfluidics-Powered Real-Time Monitoring of Isothermal DNA Amplification of Cancer Biomarker. *Biosensors* **2022**, *12*, 201. [CrossRef] [PubMed]
14. Ruan, Q.; Zou, F.; Wang, Y.; Zhang, Y.; Xu, X.; Lin, X.; Tian, T.; Zhang, H.; Zhou, L.; Zhu, Z.; et al. Sensitive, Rapid, and Automated Detection of DNA Methylation Based on Digital Microfluidics. *ACS Appl. Mater. Interfaces* **2021**, *13*, 8042–8048. [CrossRef] [PubMed]
15. Ho, K.L.; Liao, H.Y.; Liu, H.M.; Lu, Y.W.; Yeh, P.K.; Chang, J.Y.; Fan, S.K. Digital Microfluidic qPCR Cartridge for SARS-CoV-2 Detection. *Micromachines* **2022**, *13*, 196. [CrossRef] [PubMed]
16. Alias, A.B.; Chiang, C.E.; Huang, H.Y.; Lin, K.T.; Lu, P.J.; Wang, Y.W.; Wu, T.H.; Jiang, P.S.; Chen, C.A.; Yao, D.J. Extraction of Cell-free Dna from An Embryo-culture Medium Using Micro-scale Bio-reagents on Ewod. *Sci. Rep.* **2020**, *10*, 9708. [CrossRef] [PubMed]
17. Sathyanarayanan, G.; Haapala, M.; Sikanen, T. Digital Microfluidics-Enabled Analysis of Individual Variation in Liver Cytochrome P450 Activity. *Anal. Chem.* **2020**, *92*, 14693–14701. [CrossRef] [PubMed]
18. Leclerc, L.M.Y.; Soffer, G.; Kwan, D.H.; Shih, S.C.C. A fucosyltransferase inhibition assay using image-analysis and digital microfluidics. *Biomicrofluidics* **2019**, *13*, 034106. [CrossRef]
19. Peng, J.; Chan, C.; Zhang, S.; Sklavounos, A.A.; Olson, M.E.; Scott, E.Y.; Hu, Y.; Rajesh, V.; Li, B.B.; Chamberlain, M.D.; et al. All-in-One digital microfluidics pipeline for proteomic sample preparation and analysis. *Chem. Sci.* **2023**, *14*, 2887–2900. [CrossRef] [PubMed]
20. Guo, J.; Lin, L.; Zhao, K.; Song, Y.; Huang, M.; Zhu, Z.; Zhou, L.; Yang, C. Auto-affitech: An automated ligand binding affinity evaluation platform using digital microfluidics with a bidirectional magnetic separation method. *Lab Chip* **2020**, *20*, 1577–1585. [CrossRef] [PubMed]
21. Zhang, Y.; Liu, Y. Advances in integrated digital microfluidic platforms for point-of-care diagnosis: A review. *Sens. Diagn.* **2022**, *1*, 648–672. [CrossRef]
22. Li, D.; Liu, X.; Chai, Y.; Shan, J.; Xie, Y.; Liang, Y.; Huang, S.; Zheng, W.; Li, Z. Point-of-care blood coagulation assay enabled by printed circuit board-based digital microfluidics. *Lab Chip* **2022**, *22*, 709–716. [CrossRef] [PubMed]
23. Zhai, J.; Li, H.; Wong, A.H.; Dong, C.; Yi, S.; Jia, Y.; Mak, P.I.; Deng, C.X.; Martins, R.P. A digital microfluidic system with 3D microstructures for single-cell culture. *Microsyst. Nanoeng.* **2020**, *6*, 6. [CrossRef] [PubMed]

24. Zhai, J.; Li, C.; Li, H.; Yi, S.; Yang, N.; Miao, K.; Deng, C.; Jia, Y.; Mak, P.I.; Martins, R.P. Cancer drug screening with an on-chip multi-drug dispenser in digital microfluidics. *Lab Chip* **2021**, *21*, 4749–4759. [CrossRef] [PubMed]
25. Millington, D.; Norton, S.; Singh, R.; Sista, R.; Srinivasan, V.; Pamula, V. Digital microfluidics comes of age: High-throughput screening to bedside diagnostic testing for genetic disorders in newborns. *Expert Rev. Mol. Diagn.* **2018**, *18*, 701–712. [CrossRef] [PubMed]
26. Malinowski, R.; Parkin, I.P.; Volpe, G. Advances towards programmable droplet transport on solid surfaces and its applications. *Chem. Soc. Rev.* **2020**, *49*, 7879–7892. [CrossRef] [PubMed]
27. Zhu, Q.; Lu, Y.; Xie, S.; Luo, Z.; Shen, S.; Yan, Z.; Jin, M.; Zhou, G.; Shui, L. Intelligent droplet manipulation in electrowetting devices via capacitance-based sensing and actuation for self-adaptive digital microfluidics. *Microfluid. Nanofluid.* **2020**, *24*, 59. [CrossRef]
28. Li, C.; Zhang, K.; Wang, X.; Zhang, J.; Liu, H.; Zhou, J. Feedback control system for large scale 2D digital microfluidic platforms. *Sens. Actuators B Chem.* **2018**, *255*, 3616–3622. [CrossRef]
29. Zhang, C.; Su, Y.; Hu, S.; Jin, K.; Jie, Y.; Li, W.; Nathan, A.; Ma, H. An Impedance Sensing Platform for Monitoring Heterogeneous Connectivity and Diagnostics in Lab-on-a-Chip Systems. *ACS Omega* **2020**, *5*, 5098–5104. [CrossRef] [PubMed]
30. Min, X.; Bao, C.; Kim, W.S. Additively Manufactured Digital Microfluidic Platforms for Ion-Selective Sensing. *ACS Sens.* **2019**, *4*, 918–923. [CrossRef] [PubMed]
31. Fobel, R.; Fobel, C.; Wheeler, A.R. DropBot: An open-source digital microfluidic control system with precise control of electrostatic driving force and instantaneous drop velocity measurement. *Appl. Phys. Lett.* **2013**, *102*, 193513. [CrossRef]
32. Rui, X.; Song, S.; Wang, W.; Zhou, J. Applications of electrowetting-on-dielectric (EWOD) technology for droplet digital PCR. *Biomicrofluidics* **2020**, *14*, 061503. [CrossRef] [PubMed]
33. Jebrail, M.J.; Renzi, R.F.; Sinha, A.; Van De Vreugde, J.; Gondhalekar, C.; Ambriz, C.; Meagher, R.J.; Branda, S.S. A solvent replenishment solution for managing evaporation of biochemical reactions in air-matrix digital microfluidics devices. *Lab Chip* **2015**, *15*, 151–158. [CrossRef]
34. Perry, J.M.; Soffer, G.; Jain, R.; Shih, S.C.C. Expanding the limits towards 'one-pot' DNA assembly and transformation on a rapid-prototype microfluidic device. *Lab Chip* **2021**, *21*, 3730–3741. [CrossRef] [PubMed]
35. Guan, Y.; Tu, J.; Li, B.; Fu, J.; Zhu, M.; Chen, X.; Zhou, C. Stripped Electrode Based Electrowetting-on-Dielectric Digital Microfluidics for Precise and Controllable Parallel Microdrop Generation. *Langmuir* **2020**, *36*, 9540–9550. [CrossRef] [PubMed]
36. Sadeghi, S.; Ding, H.; Shah, G.J.; Chen, S.; Keng, P.Y.; Kim, C.J.; van Dam, R.M. On chip droplet characterization: A practical, high-sensitivity measurement of droplet impedance in digital microfluidics. *Anal. Chem.* **2012**, *84*, 1915–1923. [CrossRef] [PubMed]
37. Jin, K.; Huang, Q.; Hu, C.; Hu, S.; Li, J. A digital microfluidic system with integrated electrochemical impedance measurement arrays. *J. Phys. Conf. Ser.* **2022**, *2196*, 012005. [CrossRef]
38. Roques-Carmes, T.; Hayes, R.A.; Feenstra, B.J.; Schlangen, L.J.M. Liquid behavior inside a reflective display pixel based on electrowetting. *J. Appl. Phys.* **2004**, *95*, 4389–4396. [CrossRef]